



Seismic Behavior of SMA-Reinforced ECC Columns Under Different Axial Load Ratios

Muhammad Shoaib Khan¹

Received: 3 September 2022 / Accepted: 16 January 2023 / Published online: 2 February 2023
© The Author(s), under exclusive licence to Shiraz University 2023

Abstract

Axial compression load ratio is an important parameter and greatly influences the seismic performance of reinforced concrete columns because of permanent residual deformations and brittleness of ordinary steel and concrete, respectively. However, the combined working of shape memory alloys (SMA) and engineered cementitious composites (ECC) overcomes the problems due to the excellent properties of SMA and ECC such as self-recovering and ductile nature, respectively. This paper assesses the cyclic performance of SMA-ECC and RC columns under moderate to high axial load ratios using an experimentally calibrated and validated finite element model. Results are assessed in terms of performance criteria, performance drift limits, hysteretic response curves, skeleton backbone curves, strength deterioration and energy dissipation capacity. SMA-ECC columns substantially increase ultimate drift capacity as opposed to RC columns approximately by 1.52, 1.42, 1.46 and 1.79 times under axial load ratios of 0.2, 0.3, 0.4 and 0.5, respectively.

Keywords RC columns · SMA · ECC · Cyclic loading · Damage recovery

1 Introduction

During an earthquake, columns act as the primary element in resisting seismic forces. The damages of reinforced concrete (RC) frame structures during seismic activities have revealed that the poor performance of columns causes the collapse of the overall frame structure (Ye et al. 2010; Liberatore et al. 2013). Similarly, various structural failures have been reported in past earthquakes for example Kobe, 1995; Northridge, 1995; and Kashmir, 2005 due to the failure of columns. Therefore, all over the globe, researchers have been focusing to study the behavior of RC columns under seismic actions and this has been an area of practical interest.

The principal objective of modern seismic codes is ductility, i.e., structures are likely to experience damages but will not collapse and must have adequate inelastic deformation and energy dissipation capacity. However, the brittleness of the concrete consistently affects the ductility of RC columns, especially in earthquake-prone areas. To overcome the problem of concrete brittleness, the implementation of

fiber-reinforced concrete or cementitious composites is an alternative substitute to conventional reinforced concrete columns.

ECC (engineered cementitious composites) is a fiber-reinforced cement-based composite developed by Li and his co-workers (Li et al. 1993; Li and Leung 1992), and it offers excellent strain hardening, high tensile strength and ductility with multiple cracking (Leung 1996; Yu et al. 2019; Al-Dahawi et al. 2017). Various studies have been conducted in the past focused on the seismic performance of structural members built with ECC, and the results were found fruitful as opposed to the conventional concrete. For example, Fischer and Li (2002) evaluated the cyclic performance of flexural members incorporating ECC and concluded that the presence of ECC considerably increases the ductility and load-carrying capacity of the member without ties as compared to conventional concrete columns even with ties. In another study, Kawashima et al. (2011) assessed the seismic performance of ECC in the potential plastic hinge regions of bridge columns and found that the application of ECC significantly reduces the damage as opposed to the concrete columns. Additionally, Kawashima et al. (2012) investigated the performance of full-scale polypropylene ECC bridge columns under the E-Defense shake table and concluded that the use of ECC in critical locations considerably reduces

✉ Muhammad Shoaib Khan
13pwciv3995@uetpeshawar.edu.pk; shoaibuet10@gmail.com

¹ Department of Civil Engineering, University of Engineering and Technology (UET) Peshawar, Peshawar, Pakistan

the damage and the member keeps its functionality after an earthquake. In a recent study, Jia et al. (2020) evaluated the cyclic performance of bridge piers implementing polypropylene ECC in the plastic hinge regions and the authors reported a notable improvement in the seismic performance of ECC piers. Similarly, researchers have assessed the performance of ECC in other structural members and components such as beams (Yuan et al. 2014; Zhang et al. 2015; Alyousif et al. 2016; Frank et al. 2017) and beam-column joints (Said and Abdul Razak 2016; Qudah and Maalej 2014) and have demonstrated that the application of ECC leads to improvement in terms of ductility and energy dissipation capacity.

Carbon steel as a source of reinforcement in concrete structures is being used for hundreds of years. However, the major drawback of this type of steel is the low resistance to corrosion which leads to the deterioration of RC structures. To overcome this limitation, fiber-reinforced polymer (FRP) is an alternative option to steel because of its excellent corrosion-resistant properties. However, the nonexistence of yielding and inelastic branch in the stress–strain curve leads FRP RC structures to very low ductility causing brittle failure without any warning (Muntasir Billah and Shahria Alam 2012). Shape memory alloy (SMA) is a special kind of metal that recovers deformation upon the removal of loads by a property known as the superelastic effect. Additionally, SMA provides excellent resistance to corrosion and offers other key features such as high strength and good fatigue, as well as availability in many forms and arrangements (Ozbulut et al. 2011). These properties make SMA a strong contender and an alternative to regular steel for the use of reinforcement in RC structures.

In recent years, researchers have considered SMAs in various structural members and components because they improve the seismic performance of RC structures especially under large lateral loads and in earthquake-prone areas. For example, Jung et al. (2018) used NiTiNb SMA wire in the plastic hinge zone to retrofit and repair RC bridge column (designed according to the old seismic code, i.e., pre-1971) under bidirectional shake table testing and reported that SMA confinement effectively reduces the seismic damage. In another study, Nehdi et al. (2010) used NiTi SMA bar as a source of reinforcing RC beam-column joint at the plastic hinge region of the beam and reinforcing the remaining part of the beam and column with FRP. Results showed that the use of an SMA bar in the joint region shifts the plastic hinge development away from the column face as opposed to the steel-RC beam-column joint which develops a plastic hinge at the face of the column. In a study, Nahar et al. (2019) concluded that SMA-reinforced beam-column joint reduces residual strain compared to a regular steel beam-column joint, thus, minimizing the cost of rehabilitation of structures after an earthquake. Similarly, few other studies

also have been carried out on SMA shear walls (Abraik and Youssef 2018; Cortés-Puentes et al. 2018; Cortés-Puentes and Palermo 2018), as well as retrofitting of moment-resisting frames using external SMA rebars (Elbahy et al. 2019). These studies have shown that SMA improves the overall seismic performance of the system.

The implementation of smart materials SMA-ECC in structural and earthquake engineering is gaining popularity all over the globe because of their excellent properties in combination. However, SMA and ECC have been reported altogether in a few studies. For example, in a recent study, Qian et al. (2021) used an enlarging section of beams incorporating SMA rebars and ECC concrete for retrofitting purposes and observed that SMA-ECC working together significantly increases ductility by reducing deformations. Li et al. (2015) investigated the performance of SMA-ECC beams under cyclic flexural loading and noted that SMA-ECC composite system offers minimum residual deformation and recovers the damage. In another study, Cruz Noguez and Saïidi (2013) assessed the performance of SMA reinforcement and ECC grout in the plastic hinge region of the bridge column under dynamic testing. The authors reported a higher ductility and less damage in the case of the SMA-ECC composite system compared to the conventional RC column. Few other studies also have been conducted on SMA-ECC bridge columns (Hosseini et al. 2015) and shear walls (Rojas 2020). However, very limited research is available on the use of both materials working together and needs further evaluation.

Therefore, the objective of this study is to evaluate the performance of RC columns incorporating SMA and ECC as a substitute for regular steel and concrete, respectively, in the critical regions (plastic hinge location) under a combination of lateral load and different axial load ratios. The axial load ratio on the column is an important factor because it significantly reduces the ductility of the RC column when it is increased in combination with the lateral load. Axial load on column increases due to several reasons; for example, the occurrence of higher earthquake loads than the expected design, a change in the functionality use of a structure or an increase in traffic with time, etc. Thus, this paper assesses the seismic performance of smart materials SMA-ECC columns under several axial loads in terms of hysteretic response curves, performance criteria, lateral force–displacement capacity, strength/stiffness degradation and hysteretic damping.

2 Description of Considered Columns

This study considers columns of a three-story 2 by 2 bay reinforced concrete frame designed according to BCP-SP 2007 and UBC-97. The considered building was designed

for high seismicity, i.e., Zone 4 for a design PGA of 0.40 g on soil type B and was detailed according to ACI-318. Two groups of reinforced concrete columns were selected for nonlinear analysis, i.e., RC and SMA-ECC. RC group included columns reinforced with regular carbon steel and incorporating conventional concrete, while the second group comprised columns reinforced with SMA bars and incorporated ECC only in the region expecting severe damage under lateral loads (plastic hinge location). The shear span-depth ratio, materials properties and reinforcement details of both groups were considered the same. Figure 1 presents details of the considered SMA-ECC group columns. SMA as reinforcement and ECC as concrete were considered in the plastic hinge region only, while the rest of the column was reinforced with regular carbon steel and comprised normal/conventional concrete. The use of smart materials only in the plastic hinge region is ideal because they are expensive materials compared to conventional materials. Moreover, the behavior of RC columns under lateral load is generally governed by the plastic hinge region (Muntasir Billah and Shahria Alam 2012). In both groups of columns, concrete and ECC of compressive strength 27.5 MPa were selected, while the yield strength of longitudinal and transverse reinforcement of carbon steel/SMA was chosen 320 MPa. It is important to note here that initially under the application of loading, SMA reaches a point known as starting of martensite forward transformation (σ_{M_s}). This point is similar to regular steel and is the yield strength of SMA. With a further increase in loading, SMA reaches an

ultimate point called the finishing of martensite forward transformation (σ_{M_f}). Upon unloading, the stress decreases and reaches the start of austenite reverse transformation (σ_{A_s}), followed by the end of the unloading stage at the point σ_{A_f} (finishing of austenite reverse transformation). The transformation of SMA from one phase to the other is shown in Fig. 2. In the current study, FeMnAlNi SMA having 43.5–34–15–7.5 percent composition, respectively, reported by Billah and Alam (2016) was selected. The other properties of the SMA were as follows: $\sigma_{M_s} = 320$ MPa, $\sigma_{M_f} = 442.5$ MPa, $\sigma_{A_s} = 210.8$ MPa, $\sigma_{A_f} = 122$ MPa,

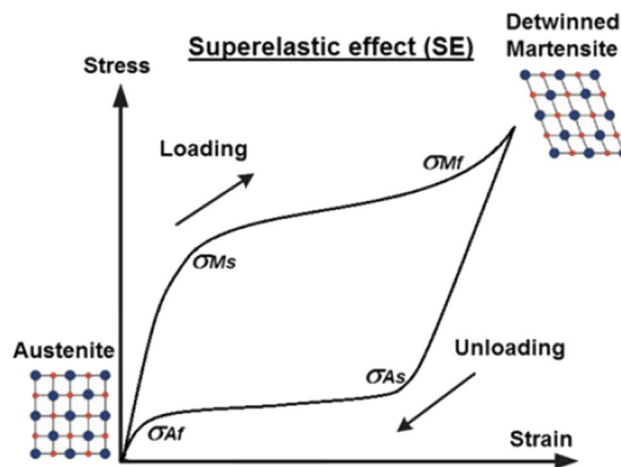


Fig. 2 Phase transformation of SMA (Fang and Wang 2019)

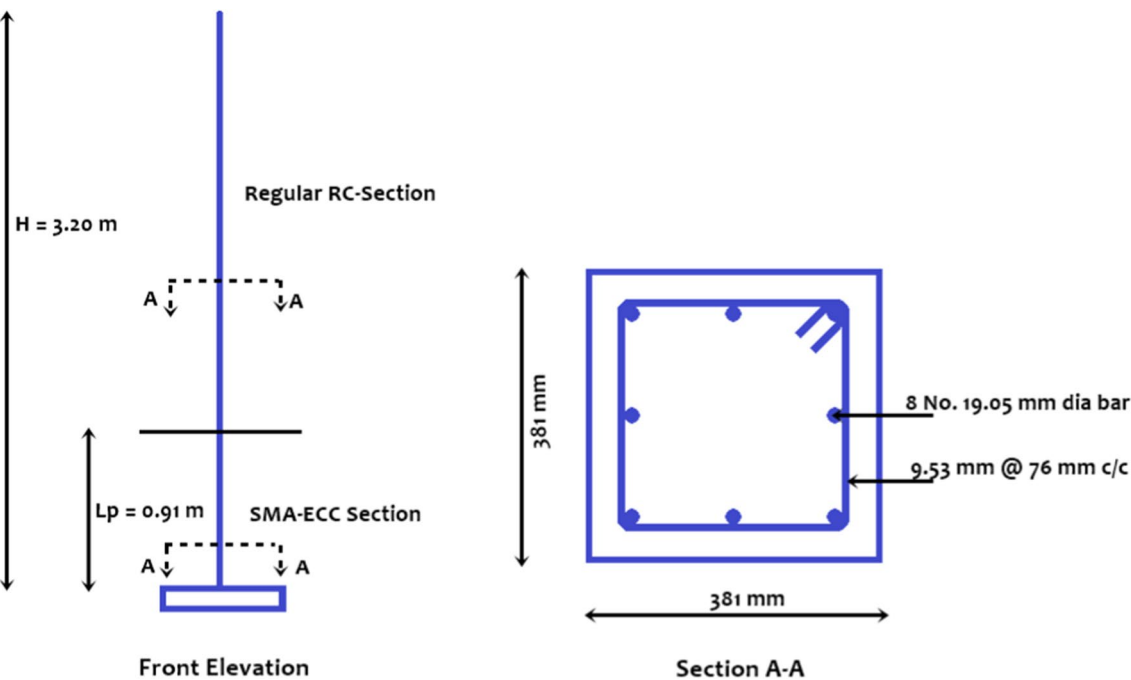


Fig. 1 Geometric and reinforcement details of SMA-ECC columns

modulus of elasticity = 98.4 GPa and superelastic plateau strain length = 6.13%.

3 Loading Protocol

Both the group of columns was analyzed under a combination of constant axial and reverse cyclic loading using the finite element-based software SeismoStruct (2020). Four different axial compression load ratios were chosen, i.e., 0.2, 0.3, 0.4 and 0.5. The axial load ratio (n) is calculated as the ratio of axial load on column (P) to the product of the gross cross-sectional area of the column (A_g) and compressive strength of concrete (f_c'), i.e. ($n = P/A_g * f_c'$). In total, eight columns were analyzed, four from the SMA-ECC group; SMA-ECC 0.2, SMA-ECC 0.3, SMA-ECC 0.4 and SMA-ECC 0.5, while four from the RC group; RC 0.2, RC 0.3, RC 0.4 and RC 0.5. The numeral 0.2, 0.3, 0.4 and 0.5 represents the axial load ratio. The axial load was applied on the top of the column fixed at the bottom, while a displacement loading protocol prepared was applied laterally as shown in Fig. 3. The displacement reversed cyclic load included two cycles of loading at each level of the run.

It is also important to define various performance criteria to relate the performance of various design alternatives, as well as post-earthquake assessment of structures.

Different performance criteria have been proposed by several researchers in terms of concrete cracking, rebar yielding, cover spalling and core concrete crushing (MacGregor and Wight 2005; Paulay and Priestley 1992; Berry and Eberhard 2003). In the present study, the cracking strain of concrete was calculated by dividing the tensile strength of concrete by the modulus of elasticity. The spalling of unconfined concrete and crushing of confined concrete were assumed to take place at a compressive strain value of 0.0045 and 0.007, respectively. A value of 0.0016 was chosen as the yielding of regular steel reinforcement bars, while the yielding of SMA was assumed to take place at a strain of 0.0032. The yield strain of SMA is different from the conventional steel due to the difference in modulus of elasticity.

4 FE-Based Numerical Modeling

Structural elements and components such as beams, columns, and beam-column joints can be modeled using mainly two methods. The first one is the concentrated plasticity approach in which the inelastic behavior is usually lumped at the end of a member in the form of a hinge or spring. The other one is the distributed plasticity approach in which either a finite length hinge zone is introduced or the entire member is divided into discrete elements further followed

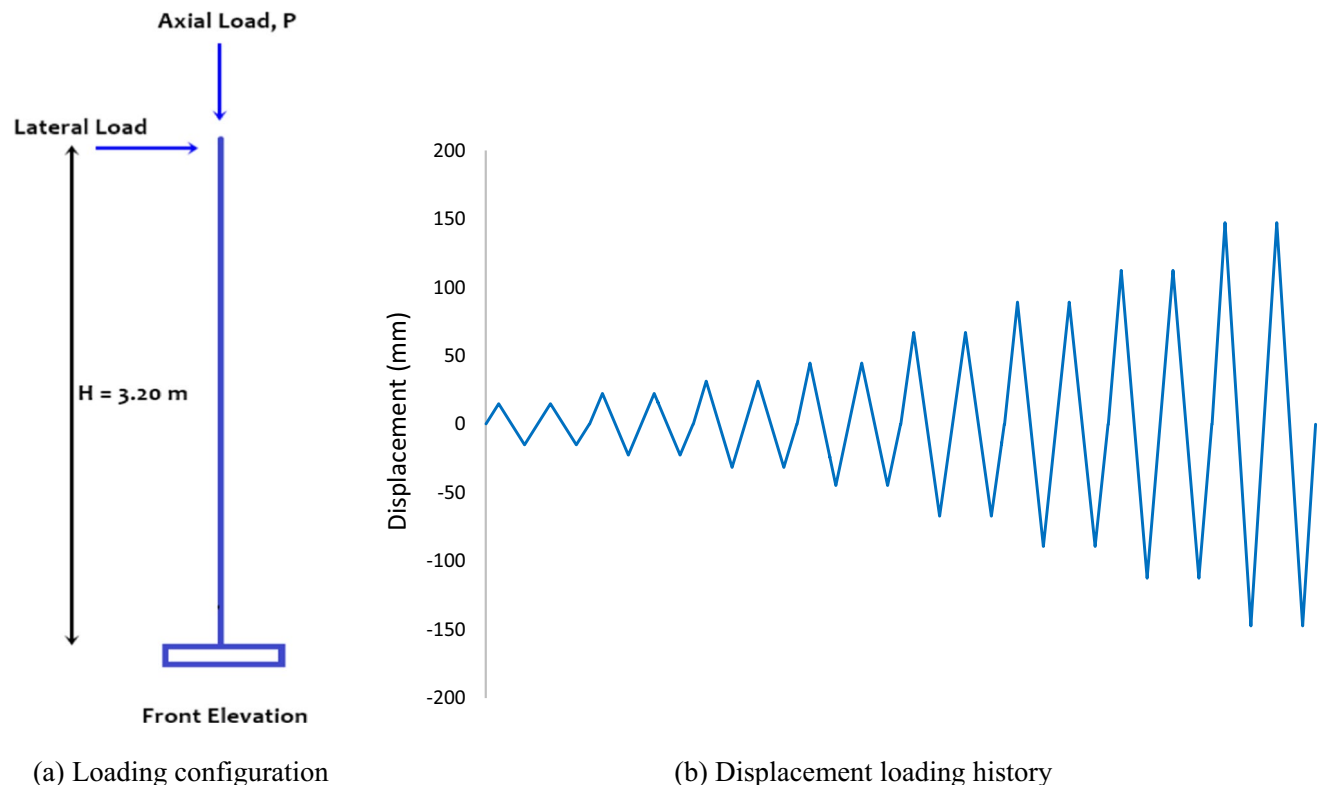


Fig. 3 Loading configuration and protocol

by cross-sectional discretization into fibers (Deierlein et al. 2010). Distributed plasticity technique has an advantage over the lumped plasticity because it simulates the complete nonlinear behavior of the member under seismic analysis. Figure 4 presents idealization details of various modeling techniques. In the present study, distributed plasticity fiber-type inelastic displacement-based element was employed to model the RC columns. Columns were divided longitudinally into three elements followed by cross-sectional discretization into 150 sectional fibers. In the fiber modeling technique, the nonlinear uniaxial stress–strain response of the individual fibers in which the entire cross section is discretized is obtained through integration. Moreover, the program SeismoStruct takes into account both geometric nonlinearities and material inelasticity and can accurately predict the large displacement and collapse load of structural members and frames under various loading protocols.

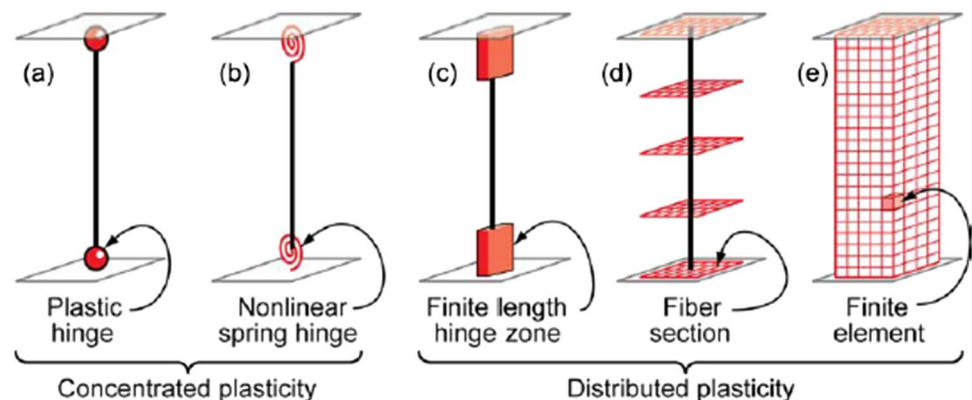
The cyclic behavior of SMA was simulated using the Auricchio and Sacco (1997) proposed SMA beam model. The model was derived on the basis of classical small deformation Euler–Bernoulli beam theory for the analysis of SMA structural members and has been programmed into the FE package by Fugazza (2003). To completely define the characteristics of this model, the parameters require are modulus of elasticity, austenite to martensite starting and finishing stress, martensite to austenite starting and finishing stress, superelastic plateau strain and specific weight. The ECC model proposed by Han et al. (2003) and the concrete model by Chang and Mander (1994) were implemented as constitutive models for simulating the confined/unconfined behavior of concrete. The parameters required for accurate modeling of ECC are as follows: cracking stress and strain, peak tensile stress and the strain at peak tensile stress, ultimate tensile and compressive strain, compressive strength and the strain at compressive strength, power for tensile and compressive unloading curves, factor for tensile and compressive unloading curves and specific weight. Similarly, parameters for the concrete model are compressive and tensile strength, strain at peak compressive and tensile stress,

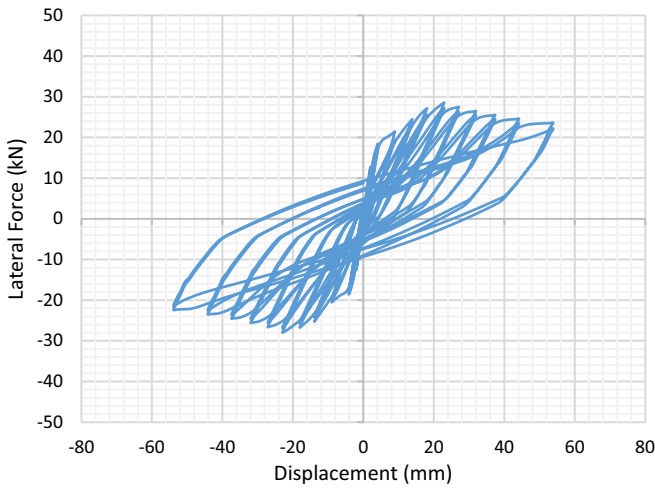
non-dimensional critical compressive and tensile strain and specific weight. The cyclic behavior of steel reinforcement was simulated using the Monti et al. (1996) programmed model, which follows the Menegotto and Pinto (1973) stress–strain relationship combined with the isotropic hardening rules of Filippou et al. (1983) and the buckling rules of Monti and Nuti (1992). This model is able to define the post-elastic buckling behavior of reinforcing bars and can simulate the response of RC members where buckling of reinforcement occurs such as in columns under severe cyclic demand. To completely define the mechanical characteristics of the material, the parameter's requirements are as follows: yield strength, modulus of elasticity, strain hardening parameter, transition curve initial shape parameter, transition curve shape calibrating coefficients, kinematic/isotropic weighting coefficient, Spurious unloading corrective parameter, fracture stain and specific weight.

5 Validation of FEM

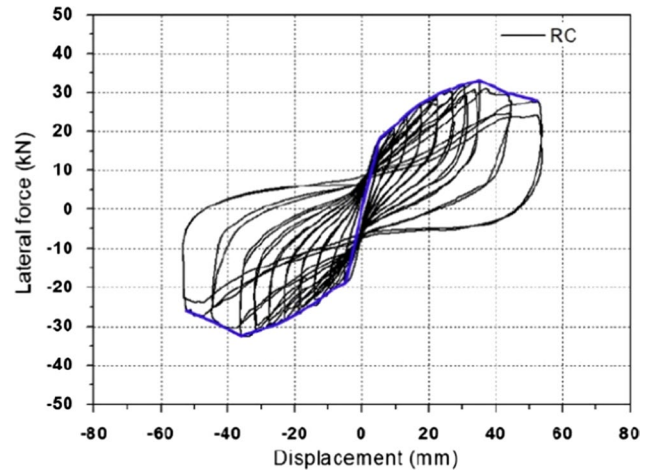
The aforementioned material models and the modeling technique were evaluated and validated with the literature available experimental data of conventional concrete/ECC columns and SMA-ECC beam. Hyun et al. (2021) investigated the behavior of RC and ECC columns under reversed cyclic and constant axial load. The tested columns were modeled using the above-mentioned modeling technique. Figure 5 presents a comparison of the simulated and tested hysteretic response curves. In the case of the RC specimen, the authors reported peak lateral resistance of 32.2 kN, while the predicted results from the FE analysis showed peak lateral resistance of 28.5 kN. On the other hand, the ECC column exhibited maximum lateral resistance of 39.1 kN during testing and is measured 37 kN in the case of FE analysis. In another study, Hung et al. (2016) tested the SMA-ECC cantilever beam under cyclic loading and the behavior of the beam was simulated using the FE analysis. Figure 6 shows the comparison of experimental and simulated force-drift

Fig. 4 Idealization of elements modeling

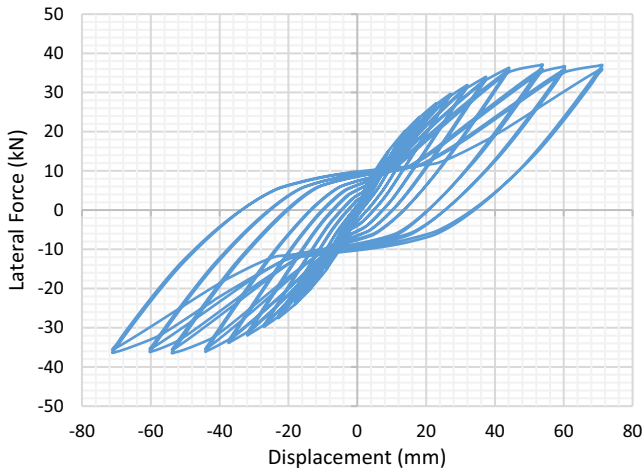




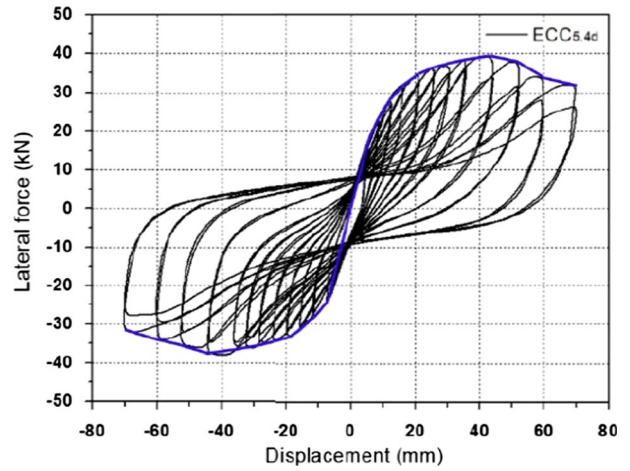
(a) FE analysis results of RC column



(b) Experimental results of RC column

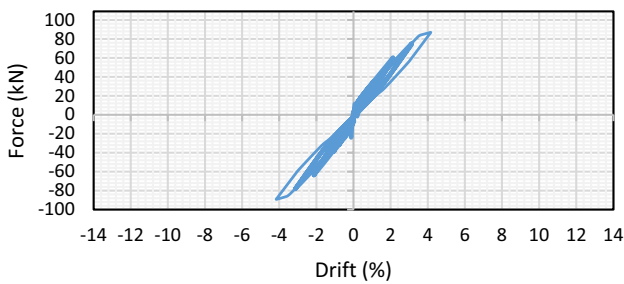


(a) FE analysis results of ECC column

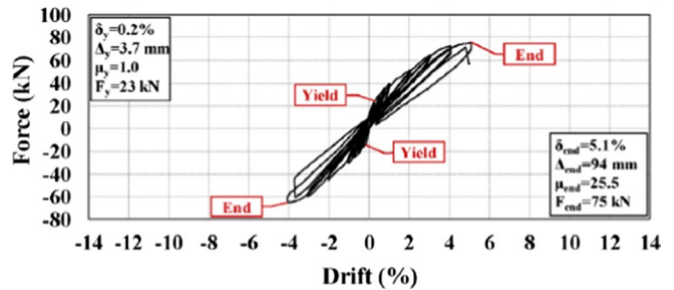


(b) Experimental results of ECC column

Fig. 5 Comparison of simulated and experimental (Hyun et al. 2021) hysteresis curves



(a) FE analysis results of SMA-ECC beam



(b) Experimental results of SMA-ECC beam

Fig. 6 Comparison of simulated and experimental (Hung et al. 2016) hysteresis curves

hysteretic curves. In the case of the tested beam, the authors reported maximum lateral resistance of 75 kN which is measured 86 kN from the FE analysis. Overall, the simulated results are in reasonable agreement with the experimental results indicating the accuracy of the modeling technique and FE package.

6 Results and Discussion

Static time history analyses were performed on both groups of columns (SMA-ECC and RC), and this section describes the results obtained.

6.1 Performance Criteria and Damage State

The damages were identified by the FE package once the strain limits (concrete cracking, spalling, core crushing and rebar yielding) defined reached the specified values. Table 1 reports the damage scale framework of both SMA-ECC and RC columns. The cracking of concrete (defined in terms of tensile strain) is initiated in RC columns earlier compared to the SMA-ECC columns due to the higher tensile strength of ECC. However, the base shear force at the cracking of ECC concrete is less than the cracking of concrete. This is reasonable because the absence of coarse aggregate in ECC concrete causes lower initial elastic stiffness as opposed to the concrete. Moreover, with the increase in axial load, the cracking of concrete occurred relatively at a slightly higher displacement drift and force in both RC and SMA-ECC columns. This is due to the increased initial integrity of the columns which improves with an upsurge in axial load. Beyond the elastic limit, the behavior of RC and SMA-ECC columns considerably changed. As evident from Table 1, the yielding of reinforcement in all RC columns occurred earlier than in SMA-ECC columns. This is because SMA has a lower modulus of elasticity compared to regular steel. The yielding of reinforcement in columns RC 0.2, RC 0.3 and RC 0.4 occurred before the initiation of spalling of concrete.

However, in the case of column RC 0.5, spalling occurred earlier than rebar yielding. A similar trend was observed for SMA-ECC 0.2, 0.3 and 0.4 columns where the yielding of longitudinal rebar occurred before the spalling of cover concrete but spalling was noted earlier than rebar yielding in the case of SMA-ECC 0.5. This is due to the deterioration of concrete which increases as the axial load is increased. Similarly, the crushing of confined concrete occurred earlier (at smaller displacement drift) as the axial compression ratio was increased for both RC and SMA-ECC columns. However, the excellent properties of ECC and SMA such as high shear strength and reduced residual deformations ability, respectively, improved the ultimate drift capacity (core crushing) of SMA-ECC columns considerably as opposed to the RC columns. For example, the ultimate lateral drift capacity of column RC 0.2 is 94.4 mm which is substantially improved in the case of column SMA-ECC 0.2–144 mm.

In the performance-based seismic design, defining various limit states (damage states) that are observable in a structure is a vital step. Various guidelines are available for defining different performance limits in terms of several engineering demand parameters such as concrete and steel strain, ductility and maximum drift (Applied Technology Council 1996; Vision 2000; Prestandard and commentary for the seismic rehabilitation of buildings. 2000). In the current study, a damage state framework is established based on three performance levels, i.e., immediate occupancy, life safety and collapse limit states. Crushing of core (confined) concrete is the stage at which the member experiences extensive damage and is near the collapsed state. In the present study, the crushing of core concrete is considered as the drift at which the columns were at the collapse level. The life safety limit is taken as 75% of the collapse level drift because at this drift, the columns experienced both spalling of concrete and yielding of rebar except for RC 0.5 and SMA-ECC 0.5 in which only spalling of concrete was noted because the increased axial load deteriorated the concrete earlier. Immediate occupancy is considered as the drift limit state at which cracking in the columns was initiated. Immediate occupancy drift

Table 1 Comparative performance of RC and SMA-ECC columns

No.	Concrete cracking		Rebar yielding		Spalling		Crushing	
	Disp (mm)	Force (kN)	Disp (mm)	Force (kN)	Disp (mm)	Force (kN)	Disp (mm)	Force (kN)
RC 0.2	7.5	25	31.5	50	65.7	45	94.4	26
RC 0.3	10.5	32	35.7	51	49.6	42	74.9	21
RC 0.4	14.1	37	38.4	44	41.1	41	64.4	17
RC0.5	19.3	47	37.5	34	32.2	40	44.7	23
SMA-ECC 0.2	14.7	17	71.3	48	65.7	48	144	36
SMA-ECC 0.3	20.7	21	80.3	43	52.3	40	107	34
SMA-ECC 0.4	27.7	23	87.4	31	44.7	33	94.4	27
SMA-ECC 0.5	34	23	85.6	15	38.4	24	80	19

limit is the level at which the columns experienced minor damage, while life safety is the performance level at which the damage is irreparable, followed by the collapse limit state. Table 2 presents the damage scale developed for both RC and SMA-ECC columns. The drift at which SMA-ECC columns reached the life safety level at a particular axial load ratio is even more than the drift at which RC columns collapsed. Moreover, the ultimate (collapse) drift capacity of SMA-ECC 0.2, SMA-ECC 0.3, SMA-ECC 0.4 and SMA-ECC 0.5 is approximately 1.52, 1.42, 1.46 and 1.79 times higher, respectively, compared to RC 0.2, RC 0.3 RC 0.4 and RC 0.5, respectively. Overall, the combined working of SMA-ECC significantly enhanced the performance of columns and ultimately improved the ductility by increasing the collapse drift capacity.

6.2 Hysteretic Response Curves

Figure 7 reports the lateral force–displacement hysteretic response curves of RC columns. The increase in axial load significantly reduces the ultimate lateral displacement drift capacity of the columns and the failure is more brittle because of the brittleness of the concrete. With the increase in axial load, the columns reached the failure stage (crushing of core concrete) rapidly after achieving peak strength. Furthermore, the peak lateral resistance in the case of RC 0.2, RC 0.3, RC 0.4 and RC 0.5 is approximately 52 kN, 53 kN, 51 kN and 47 kN, respectively. However, as the axial load increased, the columns showed maximum lateral resistance at smaller displacement drift. For example, RC 0.2 exhibited peak resistance at 43 mm displacement drift, while RC 0.3 showed peak resistance at 35 mm. Similarly, peak resistance occurred at 26 mm displacement in the case of RC 0.4 and occurred at a reduced displacement of 21 mm for the column RC 0.5.

A similar trend has been observed for SMA-ECC columns with an increase in axial load (Fig. 8). The peak resistance in

the case of SMA-ECC 0.2, SMA-ECC 0.3, SMA-ECC 0.4 and SMA-ECC 0.5 occurs at 85 mm, 82 mm, 67 mm and 53 mm, respectively. The lateral capacity of SMA-ECC 0.2, SMA-ECC 0.3, SMA-ECC 0.4 and SMA-ECC 0.5 is 49 kN, 43 kN, 35 kN and 28 kN, respectively. Under the considered axial load ratios of 0.2, 0.3, 0.4 and 0.5, the load capacity of RC columns is higher than the SMA-ECC columns by approximately 1.07, 1.24, 1.46 and 1.68 times, respectively. However, the drift capacity of SMA-ECC columns (0.2, 0.3, 0.4 and 0.5) at which the ultimate peak resistance is achieved is considerably higher than RC columns approximately by amount of 1.98, 2.34, 2.57 and 2.52 times, respectively. This means that SMA-ECC can improve the ductility of columns even under higher axial load ratios. Moreover, the hysteretic response curves of SMA-ECC columns are flag-shaped because of the flag-shaped stress–strain curve of SMA.

6.3 Lateral Force–Displacement Curves

The ultimate displacement and the corresponding base shear force under positive and negative loading cycles of each run were calculated from the hysteresis curves and were plotted to obtain the skeleton backbone curves. Figure 9 presents the skeleton backbone curves of RC and SMA-ECC columns. It is evident from the figure that the initial stiffness of RC columns is almost similar under the considered axial load ratios. On the other hand, SMA-ECC columns show a reduction in the initial stiffness as the axial load is increased. However, after reaching the peak lateral resistance, the strength and stiffness degradation occurs slowly in the case of SMA-ECC columns as opposed to RC columns. This improved performance after peak lateral resistance of SMA-ECC columns is due to the self-recovering ability of SMA which reduces the residual deformations, as well as the excellent tensile properties of ECC, leading to significant enhancement of ductility compared to RC columns.

Figure 10 shows the comparison of RC and SMA-ECC columns under the identical level of axial load ratio. From the figure, it can be seen that the stiffness before the peak resistance and the peak load capacity of RC columns is substantially higher than SMA-ECC columns as the axial load ratio is increased. This is because the modulus of elasticity of regular steel is higher than the SMA. For example, in the present study, the modulus of elasticity of the considered SMA and steel is 98.4 GPa and 200 GPa, respectively. Moreover, the absence of coarse aggregates in the ECC also causes lower elastic stiffness and thus led to reduced stiffness before peak load capacity in all SMA-ECC columns. Overall, the ultimate displacement drift capacity of SMA-ECC columns is higher than the RC columns, and the combined working of SMA-ECC avoids collapse by increasing the ultimate drift capacity.

Table 2 Drift limits of RC and SMA-ECC columns

No.	Performance levels		
	Immediate occupancy	Life safety	Collapse
	Drift %	Drift %	Drift %
RC 0.2	0.23	2.21	2.94
SMA-ECC 0.2	0.45	3.37	4.49
RC 0.3	0.32	1.75	2.34
SMA-ECC 0.3	0.64	2.50	3.34
RC 0.4	0.44	1.50	2.01
SMA-ECC 0.4	0.86	2.21	2.94
RC 0.5	0.60	1.04	1.39
SMA-ECC 0.5	1.06	1.87	2.49

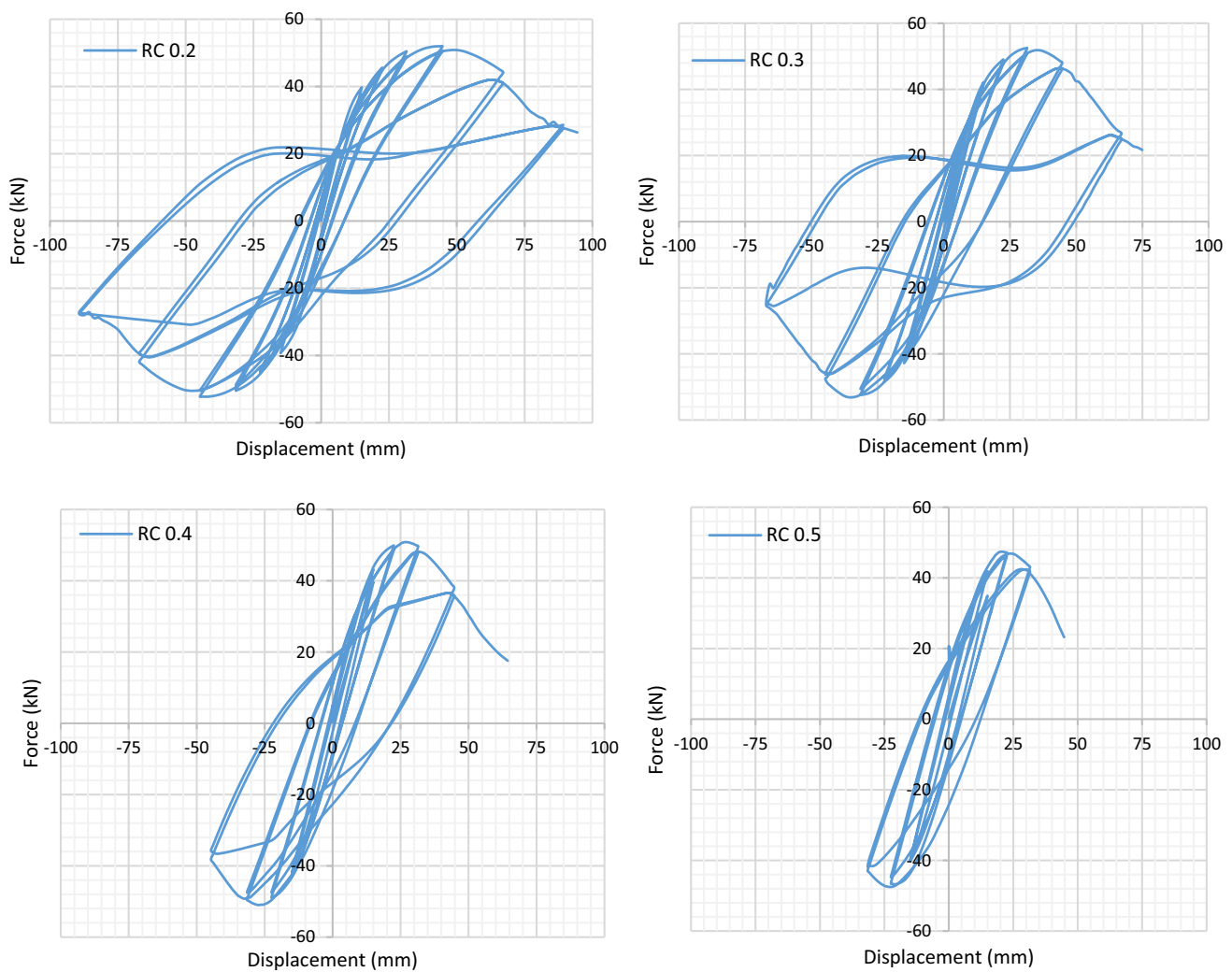


Fig. 7 Hysteretic response curves of RC columns

6.4 Strength Degradation

Figure 11 presents the strength deterioration coefficient against the lateral displacement drift for both RC and SMA-ECC columns. Strength deterioration coefficient is a factor used to describe the strength degradation of columns under cyclic loading. It is defined as the ratio of the peak lateral load in the second cycle to the peak lateral load in the first cycle of hysteresis loops. 1 represents the situation in which no strength degradation occurs and the value decreases below 1 as the column experiences strength deterioration. With the increase in axial load ratio, the graphs follow a declining trend under increasing lateral displacement demand, i.e., the deterioration coefficient of both RC and SMA-ECC columns is lower with increasing drift indicating damage and deterioration of the columns.

Damage and degradation in the case of RC columns are substantially higher as compared to the SMA-ECC columns as shown in Fig. 12. For example, under 0.2 axial load ratio, the deterioration coefficient for the RC column at 89 mm displacement (which was the ultimate loading run) is 0.67, however, at the same displacement level, the deterioration coefficient for the SMA-ECC column is 0.97. This means that the strength degradation increased in the case of the RC column approximately by 1.44 times at 89 mm loading run. Similarly, it can be seen from the curves that the deterioration coefficient for RC columns decreases more rapidly as opposed to the SMA-ECC columns during the post-peak stages due to the brittle nature of the concrete and permanent unrecoverable deformations of carbon steel. Less damage and strength degradation will reduce the cost of rehabilitation of columns after an earthquake.

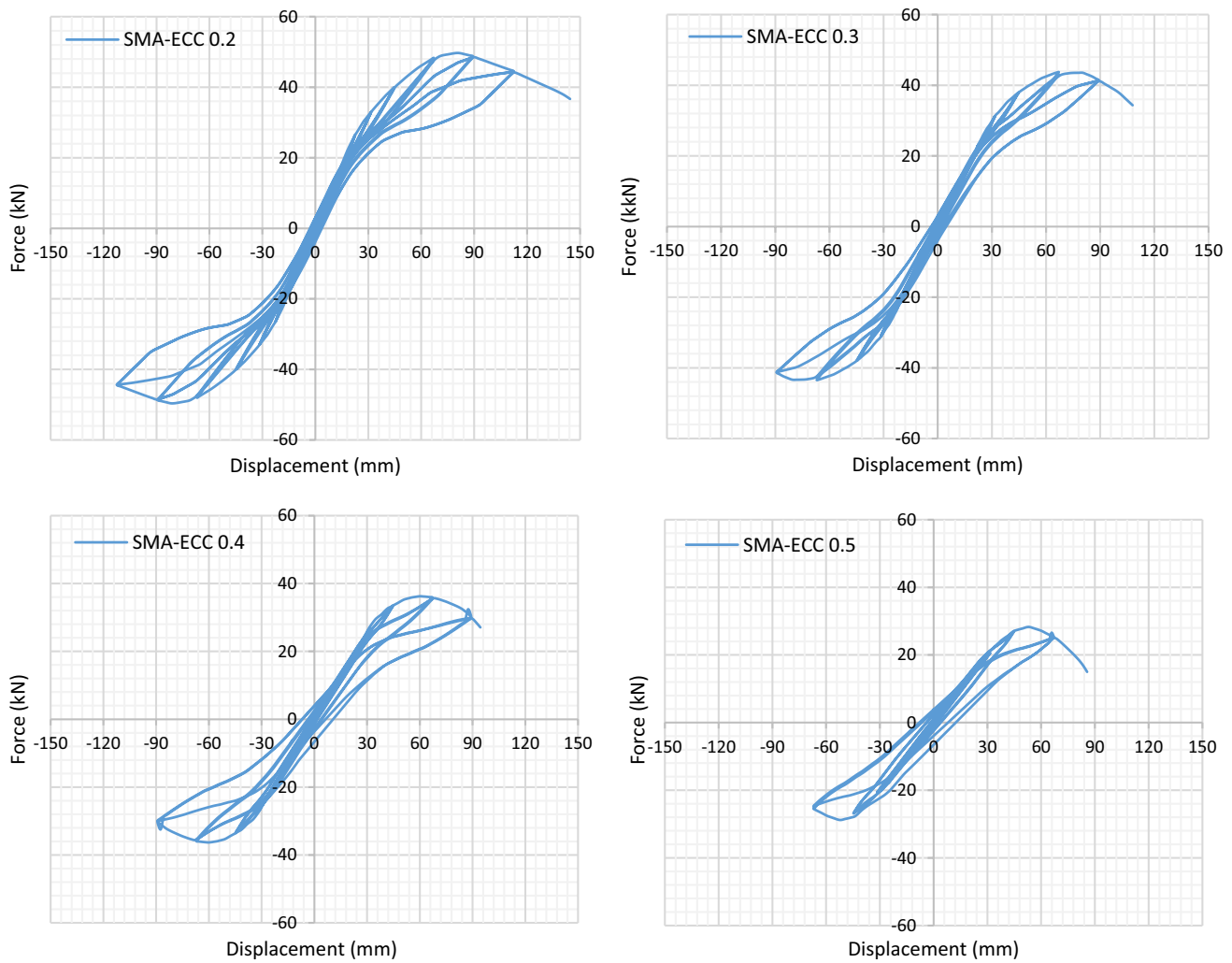


Fig. 8 Hysteretic response curves of SMA-ECC columns

6.5 Hysteretic Damping

The idea of dissipated energy (E_{diss}) in a cycle to input energy (E_{in}) has been used for the determination of hysteretic damping (ξ_{hyst});

$$\xi_{hyst} = \frac{E_{diss}}{2\pi E_{in}} \quad (1)$$

E_{diss} was measured by calculating the total area under the hysteretic cycle using the trapezoidal rule, while E_{in} was measured by calculating the area of the equivalent elastic response of the system. Figure 13 reports the hysteretic damping versus lateral displacement curves of both RC and SMA-ECC columns. It is evident from the figure that the hysteretic damping follows an increasing trend with an increase in axial load ratio in the case of all columns. For example, under 31.5 mm lateral displacement,

the hysteretic damping in the case of RC columns is as follows: 6.76% for RC 0.2, 9.47% for RC 0.3, 12.63% for RC 0.4 and 16.92% for RC 0.5. Furthermore, the hysteretic damping substantially decreased in the case of SMA-ECC columns as opposed to RC columns. For example, under the 0.3 axial load ratio, the hysteretic damping at 67 mm lateral displacement demand for the RC column is 23.87% and decreased under the same displacement level in the case of the SMA-ECC column to 2.63%. This is reasonable because of the flag-shaped stress–strain curve of SMA which offers self-recovering property.

7 Summary and Conclusions

This paper evaluated the seismic performance of RC and SMA-ECC columns under moderate to high axial load ratios. Results were assessed in terms of performance criteria, drift

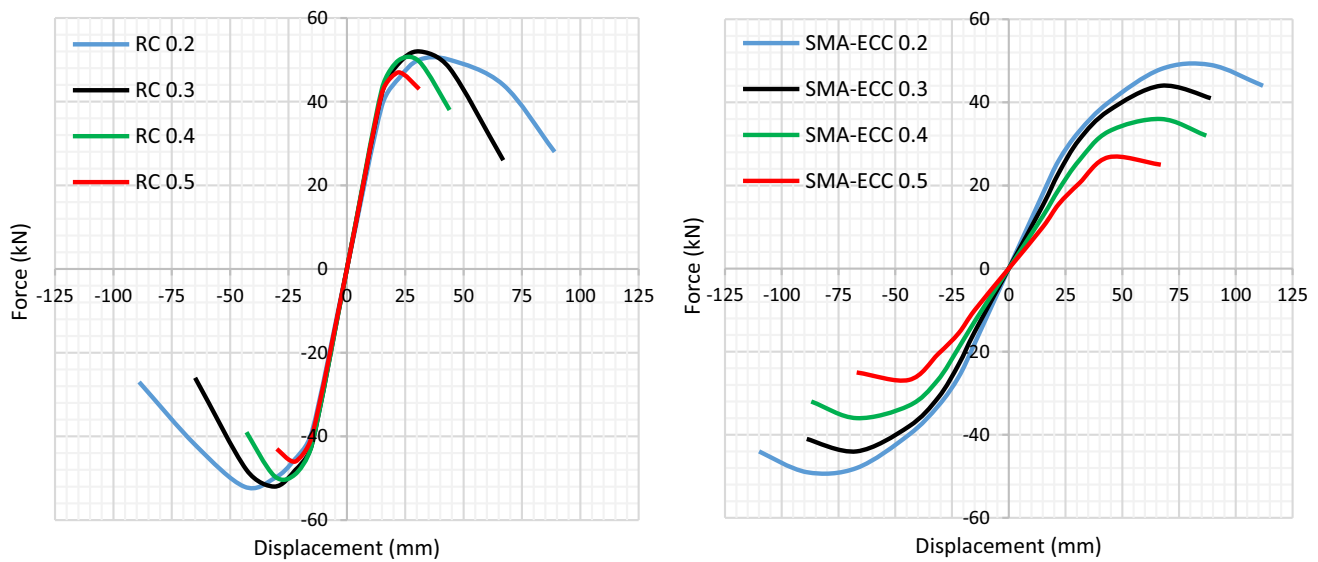


Fig. 9 Effect of axial load ratio on the backbone envelope of RC and SMA-ECC columns

limits, hysteretic response curves, lateral force–displacement curves, strength degradation and hysteretic damping. Based on the results obtained, the following conclusions are drawn;

- Under lateral loading, the axial load ratio on reinforced concrete columns greatly influences the ductility and ultimate drift capacity. With an increase in axial load, columns reach collapse level at lower lateral displacement demand.
- SMA-ECC considerably enhances the ultimate drift capacity of columns as opposed to RC columns. Under axial load ratios of 0.2, 0.3, 0.4 and 0.5, SMA-ECC improved the collapse capacity compared to RC columns by approximately 1.52, 1.42, 1.46 and 1.79 times, respectively.
- On the other hand, RC columns exhibit higher peak lateral resistance compared to SMA-ECC columns. RC columns enhanced the maximum lateral resistance approximately by 1.07, 1.24, 1.46 and 1.68 times compared to SMA-ECC columns under axial load ratios of 0.2, 0.3, 0.4 and 0.5, respectively. Moreover, the stiffness of SMA-ECC columns is also lower than RC columns.
- The maximum lateral resistance and stiffness of SMA-ECC columns can be improved by increasing the modulus of elasticity of SMA which is substantially lower than regular steel. The introduction of new elements in the composition of SMA will overcome the problem.
- Primarily, the self-recovering ability of SMA, as well as the excellent tensile properties of ECC, reduces the strength degradation in SMA-ECC columns compared to RC columns where residual deformations of carbon steel and the brittle nature of normal concrete cause significant strength deterioration. Thus, structural members built with SMA and ECC will require very less maintenance and rehabilitation cost after an earthquake.
- Hysteretic damping increases with an increase in axial load ratio. However, the hysteretic damping of SMA-ECC columns is noticeably lower than RC columns due to the flag-shaped stress–strain curve of SMA.
- The combined working of innovative materials SMA-ECC greatly improves the collapse capacity and reliability of reinforced concrete columns under different axial load ratios. The excellent self-recovering ability of SMA, as well as the good toughness, and cracking characteristics of ECC make these advanced materials an excellent alternative to ordinary steel bars and concrete in earthquake-prone areas.

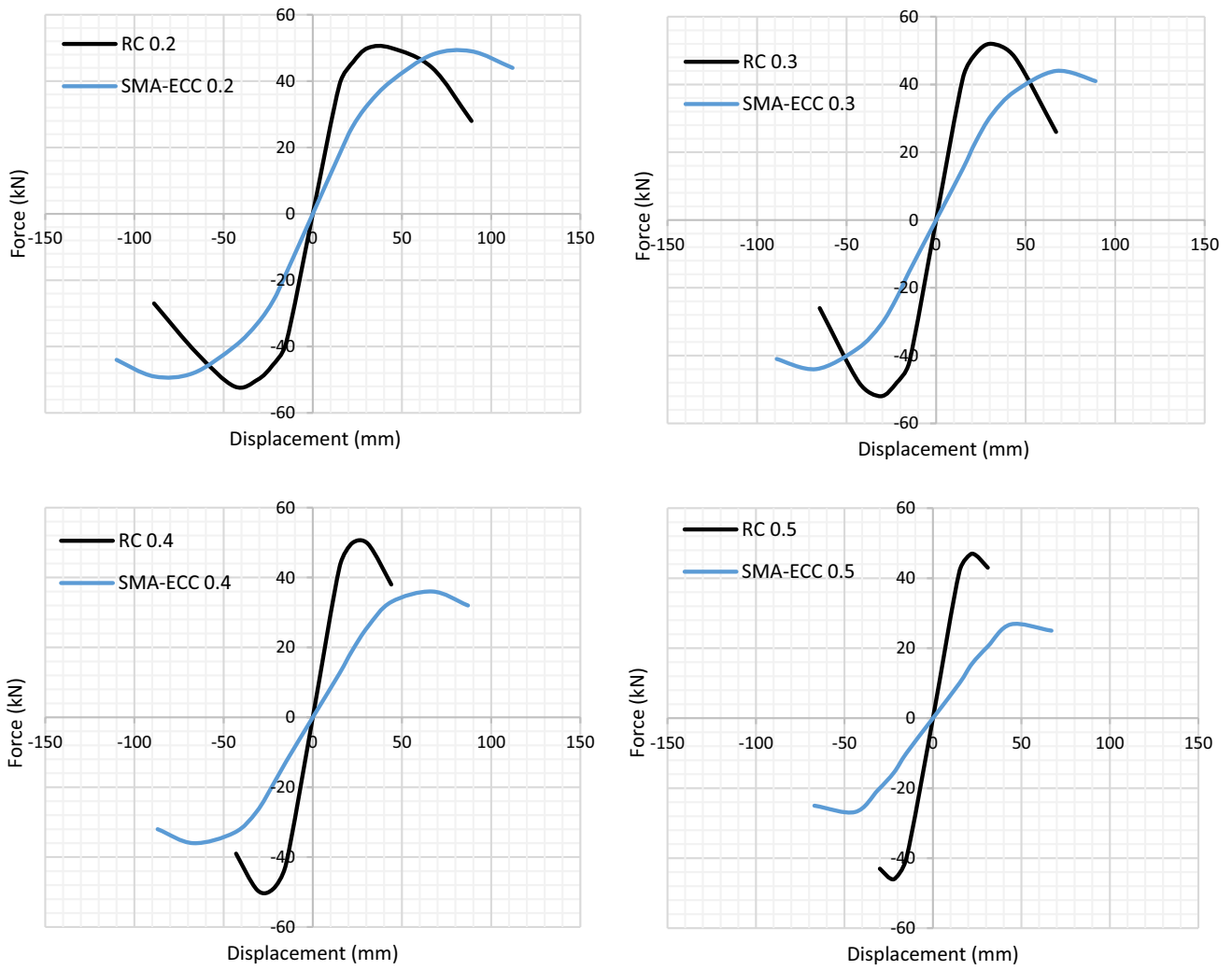


Fig. 10 Backbone comparison of RC and SMA-ECC columns under axial load ratios

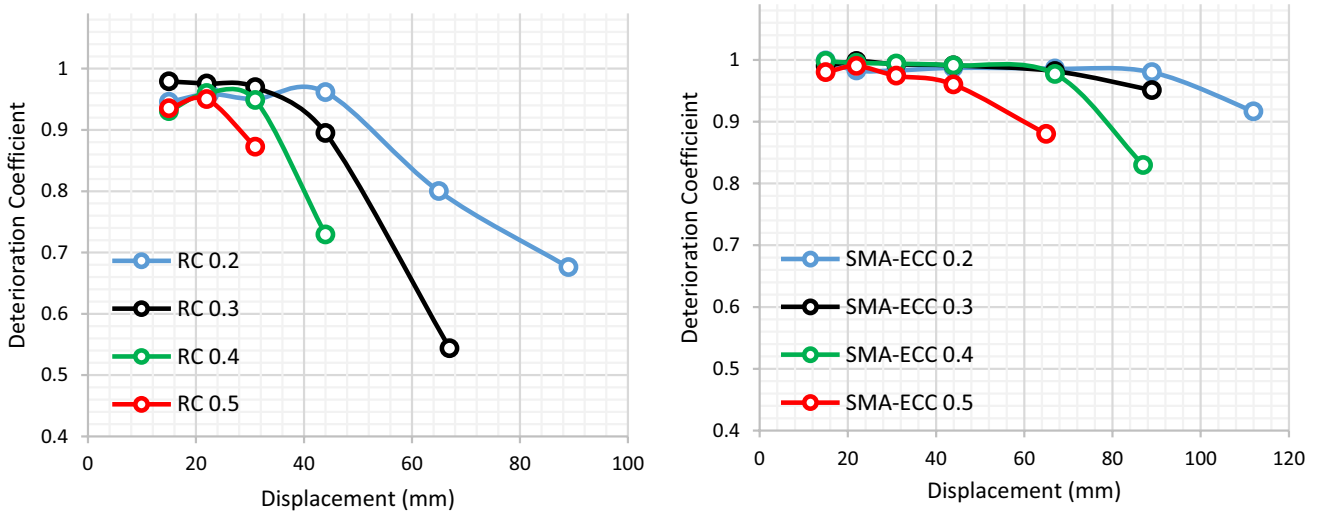


Fig. 11 Effect of axial load ratio on the strength deterioration of RC and SMA-ECC columns

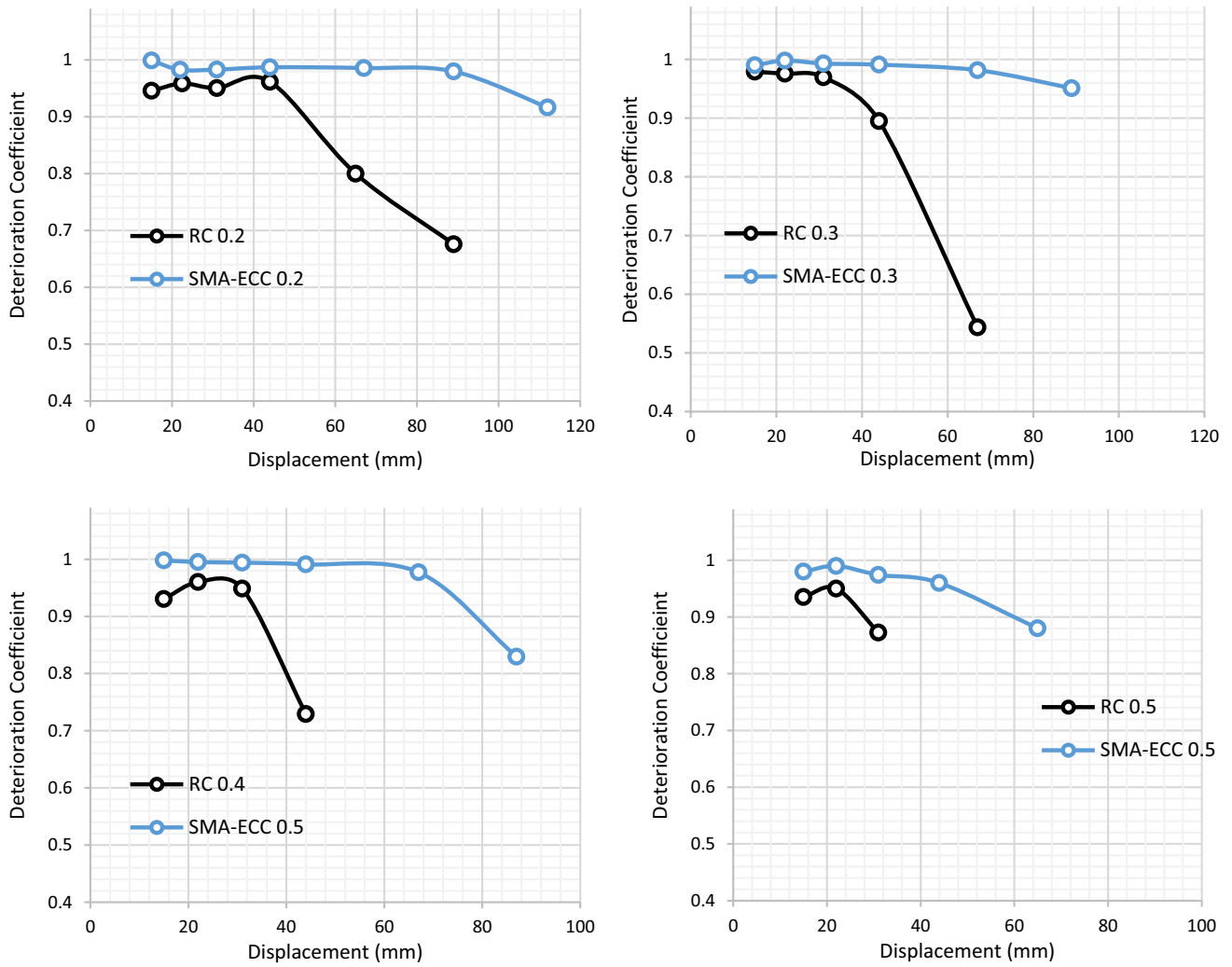


Fig. 12 Strength deterioration comparison of RC and SMA-ECC columns under axial load ratios

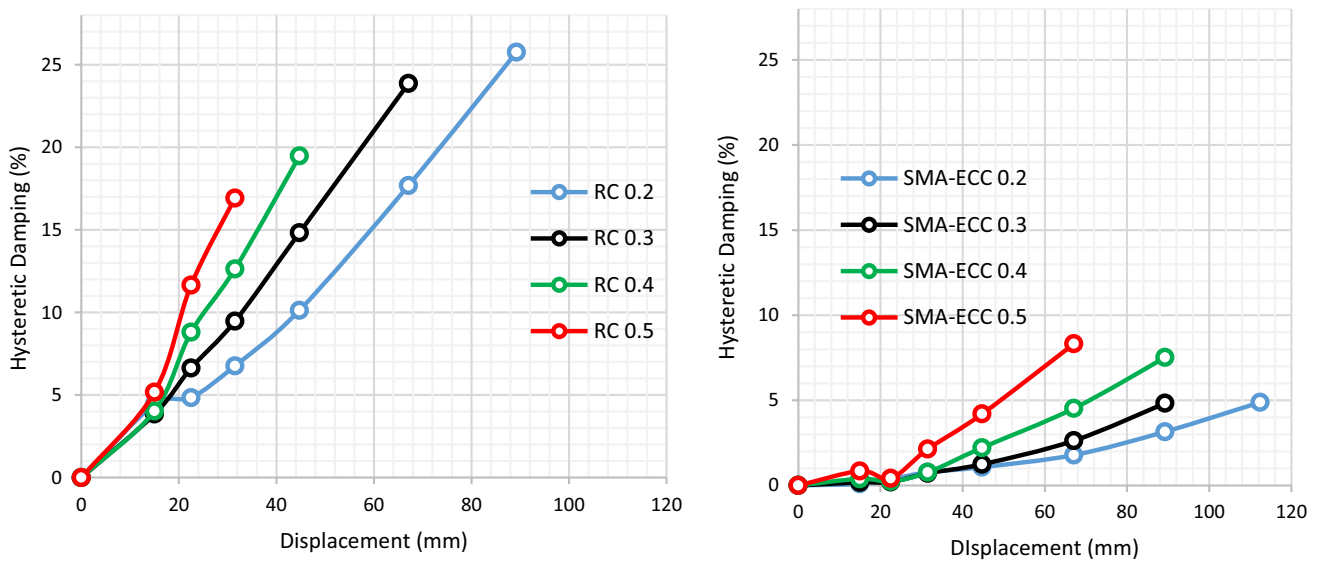


Fig. 13 Influence of axial load ratio on hysteretic damping

Acknowledgements The author is grateful to the anonymous reviewers for the review of the manuscript.

Funding This research received no funding from any funding agency.

Declarations

Conflict of interest The author declares no potential conflicts of interest with respect to the research and/or publication of this article.

References

- Abraik E, Youssef MA (2018) Seismic fragility assessment of super-elastic shape memory alloy reinforced concrete shear walls. *J Build Eng* 19:142–153. <https://doi.org/10.1016/j.jobe.2018.05.009>
- Al-Dahawi A, Yıldırım G, Öztürk O, Şahmaran M (2017) Assessment of self-sensing capability of engineered cementitious composites within the elastic and plastic ranges of cyclic flexural loading. *Constr Build Mater* 145:1–10. <https://doi.org/10.1016/j.conbuildmat.2017.03.236>
- Alyouisif A, Anil O, Sahmaran M, Lachemi M, Yıldırım G, Ashour AF (2016) Comparison of shear behaviour of engineered cementitious composite and normal concrete beams with different shear span lengths. *Mag Concr Res* 68(5):217–228. <https://doi.org/10.1680/jmacr.14.00336>
- Applied Technology Council (1996) Seismic evaluation and retrofit of concrete building ATC-40, Redwood City. Applied Technology Council (ATC), Redwood City
- Auricchio F, Sacco E (1997) A superelastic shape-memory-alloy beam model. *J Intell Mater Syst Struct* 8(6):489–501. <https://doi.org/10.1177/1045389X9700800602>
- Berry MP, Eberhard MO (2003) Performance models for flexural damage in reinforced concrete columns. Pacific Earthquake Engineering Research Center, University of California, Berkeley
- Billah AHMM, Alam MS (2016) Performance-based seismic design of shape memory alloy-reinforced concrete bridge piers. I: development of performance-based damage states. *J Struct Eng* 142(12):04016140. [https://doi.org/10.1061/\(asce\)st.1943-541x.0001458](https://doi.org/10.1061/(asce)st.1943-541x.0001458)
- Chang GA, Mander JB (1994) Seismic energy based fatigue damage analysis of bridge columns: Part 1- evaluation of seismic capacity, NCEER technical report No. NCEER-94-0006. State University of New York, Buffalo
- Cortés-Puentes WL, Palermo D (2018) Seismic retrofit of concrete shear walls with SMA tension braces. *J Struct Eng* 144(2):04017200. [https://doi.org/10.1061/\(asce\)st.1943-541x.0001936](https://doi.org/10.1061/(asce)st.1943-541x.0001936)
- Cortés-Puentes L, Zaidi M, Palermo D, Dragomirescu E (2018) Cyclic loading testing of repaired SMA and steel reinforced concrete shear walls. *Eng Struct* 168:128–141. <https://doi.org/10.1016/j.engstruct.2018.04.044>
- Cruz Noguez CA, Saiidi MS (2013) Performance of advanced materials during earthquake loading tests of a bridge system. *J Struct Eng* 139(1):144–154. [https://doi.org/10.1061/\(asce\)st.1943-541x.0000611](https://doi.org/10.1061/(asce)st.1943-541x.0000611)
- Deierlein GG, Reinhorn AM, Willford MR (2010) Nonlinear structural analysis for seismic design. NEHRP seismic design technical brief No. 4, produced by the NEHRP consultants joint venture, a partnership of the applied technology council and the consortium of universities for research in earthquake engineering, for the national institute of standards and technology, Gaithersburg, MD, NIST GCR, 10-917-5
- Elbahi YI, Youssef MA, Meshaly M (2019) Seismic performance of reinforced concrete frames retrofitted using external superelastic shape memory alloy bars. *Bull Earthq Eng* 17(2):781–802. <https://doi.org/10.1007/s10518-018-0477-7>
- Fang C, Wang W (2019) Shape memory alloys for seismic resilience. Springer, Singapore, pp 1–283. <https://doi.org/10.1007/978-981-13-7040-3>
- FEMA 356 (2000) Prestandard and commentary for the seismic rehabilitation of buildings. Federal Emergency Management Agency (FEMA), Washington
- Filippou FC, Popov EP, Bertero VV (1983) Effects of bond deterioration on hysteretic behaviour of reinforced concrete joints, report EERC 83–19, earthquake engineering research center. University of California, Berkeley
- Fischer G, Li VC (2002) Effect of matrix ductility on deformation behavior of steel reinforced ECC flexural members under reversed cyclic loading conditions. *ACI Struct J* 99(6):781–790. <https://doi.org/10.14359/12343>
- Frank TE, Lepech MD, Billington SL (2017) Experimental testing of reinforced concrete and reinforced ECC flexural members subjected to various cyclic deformation histories. *Mater Struct Mater et Constr*. <https://doi.org/10.1617/s11527-017-1102-y>
- Fugazza D (2003) Shape-memory alloy devices in earthquake engineering: mechanical properties, constitutive modelling and numerical simulations. European School of Advanced Studies in Reduction of Seismic Risk, p 148
- Han TS, Feenstra PH, Billington SL (2003) Simulation of highly ductile fiber-reinforced cement-based composite components under cyclic loading. *ACI Struct J* 100(6):749–757. <https://doi.org/10.14359/12841>
- Hosseini F, Gencturk B, Lahpour S, Gil DI (2015) An experimental investigation of innovative bridge columns with engineered cementitious composites and Cu-Al-Mn super-elastic alloys. *Smart Mater Struct* 24(8):085029. <https://doi.org/10.1088/0964-1726/24/8/085029>
- Hung CC, Yen WM, Yu KH (2016) Vulnerability and improvement of reinforced ECC flexural members under displacement reversals: experimental investigation and computational analysis. *Constr Build Mater* 107:287–298. <https://doi.org/10.1016/j.conbuildmat.2016.01.019>
- Hyun JH, Bang JW, Lee BY, Kim YY (2021) Effects of the replacement length of concrete with ecc on the cyclic behavior of reinforced concrete columns. *Materials* 14(13):3542. <https://doi.org/10.3390/ma14133542>
- Jia Y, Zhao R, Li F, Zhou Z, Wang Y, Zhan Y, Shi X (2020) Seismic performance of bridge piers constructed with PP-ECC at potential plastic hinge regions. *Materials* 13(8):1865. <https://doi.org/10.3390/MA13081865>
- Jung D, Wilcoski J, Andrawes B (2018) Bidirectional shake table testing of RC columns retrofitted and repaired with shape memory alloy spirals. *Eng Struct* 160:171–185. <https://doi.org/10.1016/j.engstruct.2017.12.046>
- Kawashima K, Zafra R, Sasaki T, Kajiwara K, Nakayama M (2011) Effect of polypropylene fiber reinforced cement composite and steel fiber reinforced concrete for enhancing the seismic performance of bridge columns. *J Earthquake Eng* 15(8):1194–1211. <https://doi.org/10.1080/13632469.2011.569051>
- Kawashima K, Zafra RG, Sasaki T, Kajiwara K, Nakayama M, Unjoh S, Sakai J, Kosa K, Takahashi Y, Yabe M (2012) Seismic performance of a full-size polypropylene fiber-reinforced cement composite bridge column based on E-defense shake table experiments. *J Earthquake Eng* 16(4):463–495. <https://doi.org/10.1080/13632469.2011.651558>
- Leung CKY (1996) Design criteria for pseudoductile fiber-reinforced composites. *J Eng Mech* 122(1):10–18

- Li VC, Leung CKY (1992) Steady-state and multiple cracking of short random fiber composites. *J Eng Mech* 118(11):2246–2264. [https://doi.org/10.1061/\(asce\)0733-9399\(1992\)118:11\(2246\)](https://doi.org/10.1061/(asce)0733-9399(1992)118:11(2246))
- Li VC, Stang H, Krenchel H (1993) Micromechanics of crack bridging in fibre-reinforced concrete. *Mater Struct* 26(8):486–494. <https://doi.org/10.1007/BF02472808>
- Li X, Li M, Song G (2015) Energy-dissipating and self-repairing SMAECC composite material system. *Smart Mater Struct*. <https://doi.org/10.1088/0964-1726/24/2/025024>
- Liberatore L, Sorrentino L, Liberatore D, Decanini LD (2013) Failure of industrial structures induced by the Emilia (Italy) 2012 earthquakes. *Eng Fail Anal* 34:629–647. <https://doi.org/10.1016/j.engfailanal.2013.02.009>
- MacGregor JG, Wight JK (2005) Reinforced concrete mechanics and design. 4th edition
- Menegotto M, Pinto PE (1973) Method of analysis for cyclically loaded R.C. plane frames including changes in geometry and nonelastic behaviour of elements under combined normal force and bending. In: Symposium on the resistance and ultimate deformability of structures acted on by well defined repeated loads, international association for bridge and structural engineering, Zurich, pp 15–22
- Monti G, Nuti C (1992) Nonlinear cyclic behavior of reinforcing bars including buckling. *J Struct Eng* 118(12):3268–3284. [https://doi.org/10.1061/\(asce\)0733-9445\(1992\)118:12\(3268\)](https://doi.org/10.1061/(asce)0733-9445(1992)118:12(3268))
- Monti G, Nuti C, Santini S (1996) CYRUS—Cyclic response of upgraded sections, report No. 96–2. University of Chieti, Italy
- Muntasir Billah AHM, Shahria Alam M (2012) Seismic performance of concrete columns reinforced with hybrid shape memory alloy (SMA) and fiber reinforced polymer (FRP) bars. *Constr Build Mater* 28(1):730–742. <https://doi.org/10.1016/j.conbuildmat.2011.10.020>
- Nahar M, Muntasir Billah AHM, Kamal HR, Islam K (2019) Numerical seismic performance evaluation of concrete beam-column joint reinforced with different super elastic shape memory alloy rebars. *Eng Struct* 194:161–172. <https://doi.org/10.1016/j.engstruct.2019.05.054>
- Nehdi M, Alam MS, Youssef MA (2010) Development of corrosion-free concrete beam-column joint with adequate seismic energy dissipation. *Eng Struct* 32(9):2518–2528. <https://doi.org/10.1016/j.engstruct.2010.04.020>
- Ozbulut OE, Hurlbaeus S, Desroches R (2011) Seismic response control using shape memory alloys: a review. *J Intell Mater Syst Struct*. <https://doi.org/10.1177/1045389X11411220>
- Paulay T, Priestley MNJ (1992) Seismic design of reinforced concrete and masonry buildings. Wiley, New York
- Qian H, Zhang Q, Zhang X, Deng E, Gao J (2021) Experimental investigation on bending behavior of existing RC beam retrofitted with SMA-ECC composites materials. *Materials* 15(1):12. <https://doi.org/10.3390/ma15010012>
- Qudah S, Maalej M (2014) Application of engineered cementitious composites (ECC) in interior beam-column connections for enhanced seismic resistance. *Eng Struct* 69:235–245. <https://doi.org/10.1016/j.engstruct.2014.03.026>
- Rojas MAS (2020) Behavior of engineered cementitious composite repaired superelastic-shape memory alloy reinforced shear walls. Master's Thesis, York University, Toronto
- Said SH, Abdul Razak H (2016) Structural behavior of RC engineered cementitious composite (ECC) exterior beam-column joints under reversed cyclic loading. *Constr Build Mater* 107:226–234. <https://doi.org/10.1016/j.conbuildmat.2016.01.001>
- Seissoft, SeismoStruct (2020) A computer program for static and dynamic nonlinear analysis of framed structures. <https://seissoft.com/>
- SEAOC (1995) Vision 2000. Performance based seismic engineering of buildings, vol. I and II: Conceptual framework. Structural Engineers Association of California, Sacramento
- Ye L, Lu X, Li Y (2010) Design objectives and collapse prevention for building structures in mega-earthquake. *Earthq Eng Eng Vib* 9(2):189–199. <https://doi.org/10.1007/s11803-010-0005-5>
- Yu KQ, Zhu WJ, Ding Y, Lu ZD, Yu JT, Xiao JZ (2019) Microstructural and mechanical properties of ultra-high performance engineered cementitious composites (UHP-ECC) incorporation of recycled fine powder (RFP). *Cem Concr Res* 124:105813. <https://doi.org/10.1016/j.cemconres.2019.105813>
- Yuan F, Pan J, Dong L, Leung CKY (2014) Mechanical behaviors of steel reinforced ECC or ECC/concrete composite beams under reversed cyclic loading. *J Mater Civ Eng* 26(8):04014047. [https://doi.org/10.1061/\(asce\)mt.1943-5533.0000935](https://doi.org/10.1061/(asce)mt.1943-5533.0000935)
- Zhang R, Matsumoto K, Hirata T, Ishizeki Y, Niwa J (2015) Application of PP-ECC in beam-column joint connections of rigid-framed railway bridges to reduce transverse reinforcements. *Eng Struct* 86:146–156. <https://doi.org/10.1016/j.engstruct.2015.01.005>

Springer Nature or its licensor (e.g. a society or other partner) holds exclusive rights to this article under a publishing agreement with the author(s) or other rightsholder(s); author self-archiving of the accepted manuscript version of this article is solely governed by the terms of such publishing agreement and applicable law.